A deep learning approach based defect visualization in pulsed thermography

Sethu Selvi Selvan[1], Sharath Delanthabettu[2,3], Menaka Murugesan[4], Venkatraman Balasubramaniam[4], Sathvik Udupa[1], Tanvi Khandelwal[1], Touqeer Mulla[1], Varun Ittigi[1]

[1]Department of Electronics and Communication, M.S. Ramaiah Institute of Technology, Bengaluru, India
[2]Centre for Imaging Technology, M.S. Ramaiah Institute of Technology, Bengaluru, India
[3]Department of Chemistry, M.S. Ramaiah Institute of Technology, Bengaluru, India
[4]Safety, Quality and Resource Management Group, Indira Gandhi Center for Atomic Research, Kalpakkam, India

Article Info

ABSTRACT

Non-destructive evaluation (NDE) is very essential in measuring the properties of materials and in turn detect flaws and irregularities. Pulsed thermography (PT) is one of the advanced NDE technique which is used for detecting and characterizing subsurface defects. Recently many methods have been reported to enhance the signal and defect visibility in PT. In this paper, a novel unsupervised deep learning-based auto-encoder (AE) approach is proposed for enhancing the signal-to-noise ratio (SNR) and visualize the defects clearly. A detailed theoretical background of AE and its application to PT is discussed. The SNR and defect detectability results are compared with the existing approaches namely, higher order statistics (HOS), principal component thermography (PCT) and partial least square regression (PLSR) thermography. Experimental results show that AE approach provides better SNR at the cost of defect detectability.

Corresponding Author:

Sethu Selvi Selvan
Department of Electronics and Communication, M.S. Ramaiah Institute of Technology
Bengaluru, Karnataka 560,054, India
Email: selvi@msrit.edu

1. INTRODUCTION

In nuclear, process and petrochemical industries regular inspection of in-service components is important to detect and characterize service induced defects. This helps in enhancing the life cycle of the component and ensures the safety of the components and the workers. Non-destructive evaluation (NDE) methods evaluate the inherent properties of materials and identify any defect or irregularity without damaging it. This not only helps in detecting defects but also predicts whether a defect is probable to occur in future or not which is a crucial factor in preventing major crisis in an industry. Deep learning approaches are widely used in the field of non-destructive testing (NDT) to enhance the signal-to-noise ratio (SNR) and thus improving the defect visibility and to measure the size and depth of defects automatically.

Pulsed thermography (PT) is one of the advanced NDE methods in which the front side of the object under inspection is exposed to a short and high energy optical pulse [1]. The front surface of the object absorbs the optical energy and converts it to thermal energy resulting in increase of surface temperature. As the rear end of the object is at ambient temperature, thermal waves diffuse from front surface to rear end causing decrease in front surface temperature. Any defect in the material alters this diffusion rate and the surface temperature above it, which is easily detected by an infrared camera [2]. It allows materials to be inspected very quickly for near-surface defects and bonding weakness. Compared to conventional techniques

like radiography and ultrasound testing, PT has advantages like non-contactless measurement and fast inspection rate, whereas the limitation is that it is confined to surface and subsurface defect detection.

Noise is an unwanted but integral part of a signal. In PT, noise is associated with the temperature response recorded in infrared (IR) camera. This noise can affect the detection of deeper and smaller defects. Reduction of such noise is essential, which can be considered as a post processing step. In PT numerous methods have been reported for reduction of noise and thus improve SNR, an important parameter which indicates the effectiveness of noise reduction. Some of the important methods based on statistical and regression-based algorithms are higher order statistics (HOS) [3], thermal signal reconstruction (TSR) [4], principal component thermography (PCT) [5], and partial least square thermography (PLST) [6]. In recent years the trend has been shifted towards neural network (NN)-based algorithms for signal enhancement. Extensive work has been reported in the field of automated detection and characterization of defects in PT [7]–[12], [13]–[18]. Various neural networks like multilayer back-propagation NN [7]–[10], [12], [13], Kohonen and perceptron based NN [11], convolutional neural network (CNN) [14] and deep feed forward NN [15]–[17] have been used for defect detection and depth quantification in materials like plastics, composites and aluminium. These algorithms provide reasonable accuracy in defect detection and depth estimation. Apart from defect depth and size estimation, improving the defect visibility by enhancing the SNR is also important. SNR enhancement using neural networks has not been explored in PT. In [18] stacked auto-encoder (AE) method was reported for enhancing the delamination visibility in composites using PT. In this approach, pre-processed temporal pixel information is used to train the neural network. The study showed that this method significantly improved the delamination contrast.

In this paper, an unsupervised AE based neural network approach is explored to enhance SNR in PT experiments for AISI 316 L Stainless Steel material and the performance is compared with other approaches, which gives one or few images as output, namely HOS, PCT, and PLST in terms of SNR and defect visibility. Similar to HOS, the output is a single image obtained from 3D raw PT data. This saves on the time for inspection, as one need not go through the complete image sequence to locate the defect.

The paper is organized as follows: section 2 provides a detailed theoretical background on PT and the existing algorithms for signal enhancement. Section 3 elaborates the proposed algorithm for enhancing PT signal and section 4 provides the comparison of the performance of the proposed algorithm with the existing algorithms. Finally, the paper is concluded and future directions for the proposed work is provided in section 5.

2. THEORETICAL BACKGROUND AND EXISTING ALGORITHMS
2.1. Pulsed thermography (PT)

In PT, a short and high-power pulse is impinged on the surface of the object under inspection. The absorption of the optical pulse by the surface of the object results in instantaneous increase in its surface temperature. The diffusion of heat then results in decrease in the surface temperature which is monitored using an IR camera. Any interference, like a defect, alters the diffusion rate, which causes a change in the surface temperature picked up by the IR camera. The signal acquired by PT is of three dimensions with spatial information (camera pixels) recorded as a function of time. If $N_x \times N_y$ is the resolution or the number of pixels captured by the IR camera and $N_t = F_r \times t$ is the total number of thermal images, where F_r is the frame rate and t is the duration of the PT experiment, then the raw PT data set is of size $N_x \times N_y \times N_t$. The schematic diagram of the PT set-up is shown in Figure 1.
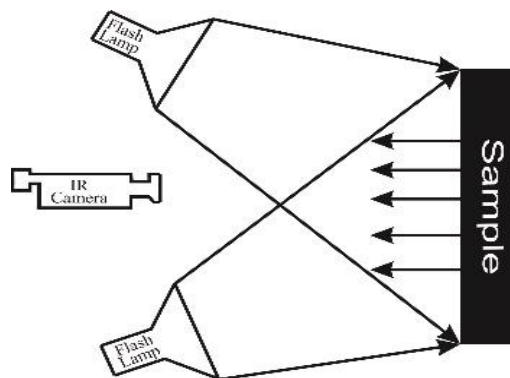

Figure 1. Schematic diagram of PT experimental set-up

2.2. Higher order statistics (HOS)

HOS analysis [3] is employed to process IR images and to compress the most useful information into a unique image for inspection. PT response with respect to time is described through its statistical behaviour. This statistical behaviour is used to analyze the different characteristics of thermal images as higher order statistical parameters have a relation to thermal conductivity in the longitudinal direction of a material. Various statistical moments such as skewness, kurtosis, hyper-skewness and hyper-flatness are considered, and these moments are then combined to form one image for each of the statistical moment. The nth standardized central moment is calculated using (1) as skewness is 3rd order central moment, kurtosis is 4th order central moment, hyper-skewness is 5th order and hyper-flatness is 6th order central moment:

$$M_n = \frac{E[(X-E[X])^n]}{\sigma^n} \tag{1}$$

where X is the data distribution, σ is the standard deviation and $E[X]$ is the mean of X. Skewness represents a measure of symmetry, or the lack of symmetry of a distribution. Kurtosis characterizes the heaviness of the tail of the distribution, compared to the normal distribution. Hyper-skewness measures the symmetry of the tails, while hyper-flatness measures similarly but with heavier focus on outliers than the fourth moment. Odd order moments quantify relative tailedness and even order moments quantify total tailedness. Standardized central moments of higher order provide larger values due to the higher power terms and cannot be defined physically as they are associated with the presence of outliers. Kurtosis and skewness are used for enhancing the defect visibility and SNR in PT.

2.3. Principal component thermography (PCT)

The temperature response signals of PT tend to be monotonic and, so oscillatory basis functions are inappropriate. This method [5] constructs a set of empirical orthogonal functions (EOF) which are statistical modes that provide the strongest projection for the data and offers a very compact representation. The thermal behavior associated with underlying defects of a material is compactly described through a singular value decomposition (SVD) of the data matrix. In general, any matrix A of size $N_x \times N_y$ can be decomposed as in (2):

$$A = USV^T \tag{2}$$

where the three matrices are: U whose columns comprise the set of EOF that models spatial variations, S is a diagonal matrix with singular values on its diagonal and rows of V^T are the principal component vectors which describe the characteristic time behaviour. The first few columns of matrix U are used to reconstruct the data to reduce the redundancy in the original data set.

Principal component analysis (PCA) applied to PT data in the form of thermogram sequence is called PCT [5] and cannot be applied directly to a 3-D thermographic data matrix. A pre-processing step of data unfolding is necessary which converts the 3D matrix of size $N_x \times N_y \times N_t$ to a 2D expanded matrix $\left((N_x \times N_y) \times N_t\right)$. The unfolded data matrix is normalized by subtracting the mean from each column divided by standard deviation of that column. The normalisation ensures that pixel to pixel variations does not influence the decomposition. PCT yields high levels of thermal contrast for underlying defects in composite materials which results in defect detection compared to conventional thermographic algorithms.

2.4. Partial least square thermography (PLST)

In contrast to PCA where the matrix U describes the variance, partial least squares regression (PLSR) [6] computes loadings (P) and scores (T) vectors that are correlated with the predicted matrix Y, which describes the variation in matrix X similar to principal component regression. The matrix X is the surface temperature matrix, while Y is the observation time of the thermal images. The result of the bilinear decomposition is a new set of thermal images and observation time vector composed of latent variables in a new subspace which considers only the most important variations.

PLSR is based on the basic latent component decomposition of X and Y matrices into a combination of loadings, scores and residuals [6]. Mathematically, the PLS model is expressed as in (3) and (4). The scores are orthogonal and are expressed as linear combinations of the original variables X with the coefficients W as expressed in (5):

$$X = TPT + E \tag{3}$$

$$Y = TQT + F \tag{4}$$

$$T = XW \tag{5}$$

where T is the score matrix, P and Q are loading or coefficient matrices and describe how the variables in T relate to the original matrices X and Y. E and F are residual matrices and represent noise or irrelevant variability in X and Y respectively.

Once the scores matrix T is obtained, the loading matrices P and Q are estimated by regression of X and Y onto T. The residual matrices E and F are found by subtracting the estimated versions of TPT and TQT from X and Y, respectively. The regression coefficients are obtained using (6) and the regression model is given as in (7).

$$B = WQT \tag{6}$$

$$Y = XB + F = XWQT + F \tag{7}$$

2.5. Deep learning based algorithms

Infrared imaging-based PT is used to automatically inspect, detect, and analyse infrared images. Passive thermography is based on visible light and is a imaging tool for self-heating objects such as the human body and electrical power devices. Active thermography is a NDT method for quality and safety evaluation of non-self-heating objects. The rapid development of deep learning makes PT more intelligent and highly automated, thus considerably increasing its range of applications. This paper [19] reviews the principle, cameras, and PT data to discuss the applications of deep learning.

In this study [20], artificial intelligence was applied in combination with infrared thermography to detect and segment defect on laminates. Segmentation was performed on both mid-wave and long-wave infrared sequences obtained during PT experiments through a deep neural network for each wavelength. The F1-score for mid-wave images based model is 92.74%, while for long-wave images is 87.39%.

In this paper [21], synthetic data from the standard finite element models (FEM) are combined with experimental data to build large datasets with mask region based convolutional neural networks (Mask-RCNN), learn essential features of objects of interest and achieve defect segmentation automatically. The results prove the efficiency of adapting inexpensive synthetic data together with the experimental dataset for training the neural networks to obtain an achievable performance from a limited collection of the annotated experimental data of a PT experiment.

In this paper [22], an artificial neural network (ANN) is employed to detect depth of the defects in composite samples, coupled with PT. The study presents a proof of concept using a Multiphysics FEM simulation model of the inspection process, to generate a training dataset and the proposed NN was further tested experimentally to validate its accuracy and performance. The accuracy of the developed NN for the synthetic data was more than 97% and for the experimental data was around 90%.

Kovács *et al.* [23] investigate two deep learning approaches to recover temperature profiles from PT images in NDT. In the first method, a deep neural network (DNN) was trained in an end-to-end fashion with surface temperature measurements as input. In the second method, the surface temperature measurements were converted to virtual waves, which was then fed to the DNN. For a dataset of 1,00,000 simulated temperature measurement images both the end-to-end and hybrid approach outperformed the baseline algorithms in terms of reconstruction accuracy. The end-to-end approach requires less domain knowledge and is computationally efficient. The hybrid approach requires extensive domain knowledge and is computationally expensive than the end-to-end approach. The virtual waves are useful features, that yields better reconstructions with the same number of training samples compared to the end-to-end approach. It also provided more compact network architectures and is suitable for NDT in two dimensions.

In [24] Fang *et al.* propose a specific depth quantifying technique by using gated recurrent units (GRUs) in composite material samples via PT. The proposed GRU model automatically quantified the depth of defects and was evaluated for accuracy and performance of synthetic carbon fiber reinforced polymer (CFRP) data from FEM for defect depth predictions. In [25], Lou *et al.* propose a spatial and temporal hybrid deep learning architecture, which has the capability to significantly minimize the uneven illumination and enhance the detection rate. The results show that Visual Geometry Group-Unet (VGG-Unet) significantly improves the contrast between the defective and non-defective regions.

3. AUTOENCODER BASED DEFECT VISUALIZATION

Neural network architectures have seen tremendous success in the past few years. CNN is one of the key architectures which performs well on a lot of tasks such as image classification and object detection. It does so by capturing the inherent features of the images in the convolution layers. The convolution layers

perform convolution operations over the image with a set of kernels, and in this case, convolution refers to Hadamard product. These layers are stacked together many times and additional methods are incorporated in between such as pooling and activation functions. These set of layers are then optimised towards a target and the loss encured is backpropagated. This process modifies the kernel weights until the loss converges. Once the architecture is optimised, the kernels capture the subtle features in the dataset and represents them in a very high dimension. The integration property of CNNs aids in feature representation.

Autoencoder is an unsupervised learning algorithm which tries to learn the function $h(x) \approx x$. A well-trained function $h(x)$ generates a new thermal image with better representation of features compared to any single input image obtained from input images used for training. The structure of the autoencoder is as shown Figure 2.
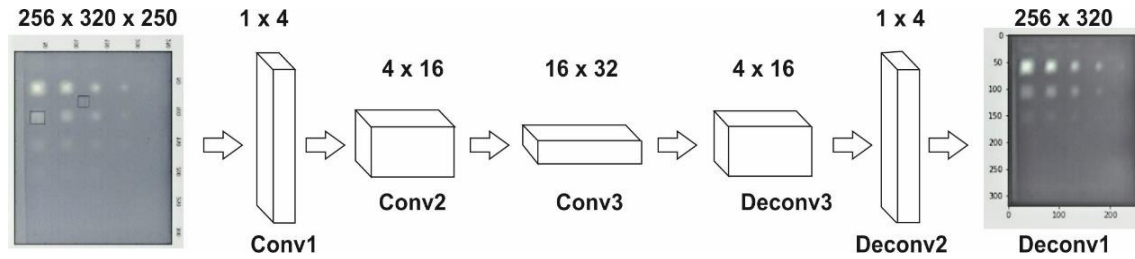
Figure 2. Autoencoder structure

In the encoder section, multiple convolution operations are applied to learn a large number of feature maps. These feature maps contain predominant information from the input images. These feature maps are reconverted back into the shape of input images in the decoder section. Training this network over the input images optimizes a loss function to output a new image with considerable SNR improvement.

The architecture consists of convolution layers denoted by $conv_i, i = 1,2,3$ and transpose convolution layers $Tconv_i, i = 1,2,3$. After each convolution layer an activation function $f(x) = ReLu(x)$ is used. In the last layer of transpose convolutions, another function $g(x) = sigmoid(x)$ is used. The convolution operation in each layer produces a feature map after it is multiplied with predefined number of kernels as shown in (8), where C_j is the feature map of layer j, C_{in} is the dimension of the input to j^{th} layer and 'weight' and 'bias' are the parameters learnt by the network. During convolution, rectified linear units (ReLu) defined in (9) are inserted as activation functions to include non-linearity and to help in loss convergence.

$$\text{output}(C_j) = \text{bias}(C_j) + \sum_{k=0}^{C_{in}-1} \text{weight}(C_j)\text{input}(k) \tag{8}$$

$$ReLu(x) = \max(0,x) \tag{9}$$

In the decoder, different transpose convolution operations are stacked which upsamples the image back to its original size. A sigmoid activation function as shown in (10) is included at the end of last layer, which squashes the values between 0 and 1 providing the probability values.

$$\sigma(x) = \frac{1}{1+e^{-x}} \tag{10}$$

To train this network, mean squared error as in (11) is used as a pixel level loss function between original and reconstructed images which employs Adam optimizer based gradient descent algorithm. Hyperparameters are chosen for loss convergence and which provides a performance exceeding a pre-defined SNR threshold.

$$L = \sum_{i=1}^{T} \sum_{m=1}^{M} \sum_{n=1}^{N} \left[x_{(m,n)}^i - y_{(m,n)}^i\right]^2 \tag{11}$$

The proposed algorithm consists of 3 layers of convolution followed by 3 layers of transpose convolution. The number of input channels vary as 1–8–16–8–1 during this process. Convolution filters of size 1×1, 2×2 and 3×3 is considered. A batch size of 4 was considered as there were less number of images for training and learning rate was set to 1×10^{-4}.

4. PERFORMANCE COMPARISON
4.1. Material
For the study, AISI 316L grade stainless steel plate of dimension 150×100×3.54 mm with artificially induced defects of size 10 mm, 8 mm, 6 mm, 4 mm and 2 mm at depths 0.4 mm, 1.13 mm, 1.78 mm, 2.48 mm, 3.17 mm, and 3.36 mm was used. The front surface of the sample was coated with black paint to improve the emissivity and light absorption. The photograph of the sample is given in Figure 3.
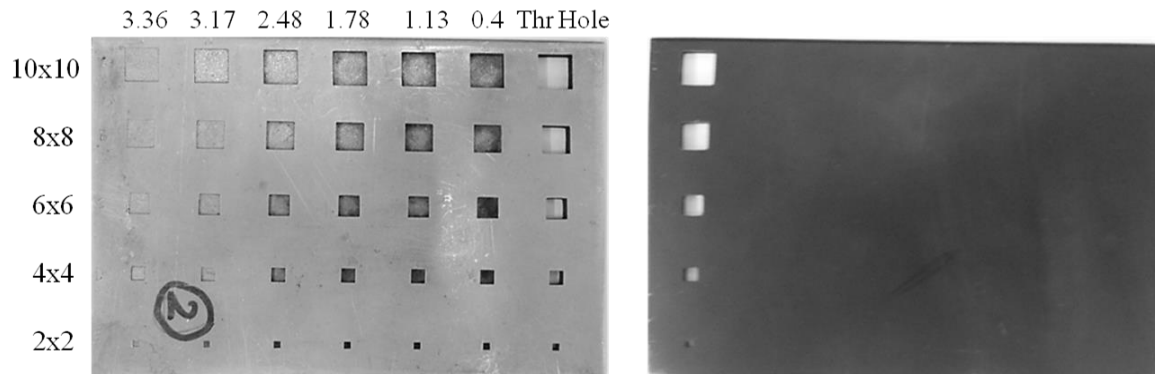

Figure 3. Photograph of a sample

4.2. Experimental set-up
CEDIP Silver 420 infrared camera was used for the experiment. The camera has a focal plane array of 320×256 pixels which is made up of Indium Antimonide (InSb) detector with Stirling cooling system. It detects the infrared radiations in 3–5μm region. The maximum achievable temperature resolution is 25 mK with a frame rate of 176 Hz. For PT experiment, two Xenon flash lamps of power 1600 W each were used. The flash duration was less than 2 ms. Experiment was carried out in reflection mode. The non-defective area temperature decreases until stabilization is reached.

4.3. Data acquisition
The thermal images acquired are stored as a 3D matrix. The spatial x- and y-coordinates correspond to the pixel locations, respectively, and the z-coordinate represents time. The acquisition frequency (fs) is 125 Hz (Sampling time t = 1/fs = 0.008s), which is the maximum full-frame rate achieved for a 256×320-pixel array. Furthermore, a total of N = 250 frames were collected during the cooling regime, where the acquisition window is t = 2s. For analysing the proposed algorithm, different defects of varying sizes and depths are considered as depicted in Table 1 and in the defect name R indicates the defect row number and C indicates the defect column number in the thermal images.

Table 1. Defects considered for analysis

Sl. No.	Defect Name	Dimensions	Depth
1.	R1C2	10×10 mm	0.4 mm
2.	R2C2	8×8 mm	0.4 mm
3.	R1C3	10×10 mm	1.13 mm
4.	R2C3	8×8 mm	1.13 mm
5.	R1C4	10×10 mm	1.78 mm
6.	R2C4	8×8 mm	1.78 mm

4.4. Higher order statistics (HOS)
The PT image is reconstructed using four different statistical moments. The SNR for different defects have been calculated and tabulated in Table 2. From the results, it is observed that maximum SNR is obtained with skewness based reconstruction in most of the defects. Kurtosis based reconstructed image also provides good SNR improvement but lower than skewness. It is also observed that hyper-skewness and hyper-flatness provide smaller SNR values than that of the unprocessed raw image.

Table 2. SNR in dB for HOS based algorithm

Sl. No.	Defect	SNR (dB)				
		Raw Image	Skewness	Kurtosis	Hyper-skewness	Hyper-flatness
1.	R1C2	32.090	37.346	32.264	24.354	22.651
2.	R1C3	20.968	27.611	27.480	17.897	16.877
3.	R2C2	33.091	36.877	32.017	22.400	22.190
4.	R2C3	18.639	11.198	6.689	18.464	17.290
5.	R3C2	31.478	37.116	32.129	23.967	22.332

4.5. Principal component thermography (PCT)

The first five components of the EOF matrix are reconstructed into 5 images along with the raw image for analysis as shown in Figure 4. These five components were extracted from the PCA of the reshaped thermal data. By extracting the most dominant features, the defects are predominantly seen in the feature space.

The principal components provide a very high contrast image with respect to the defects. This helps in clear visibility of the defects and also increases the SNR. The SNR values of six defects are tabulated for the first five principal components and then compared with the SNR values of the defects in the raw image as tabulated in Table 3. From the illustrations, it is observed that the first principal component corresponding to EOF 1 preserves more information about the defects and also visibility and contrast reduces in further components, when compared with the raw image.
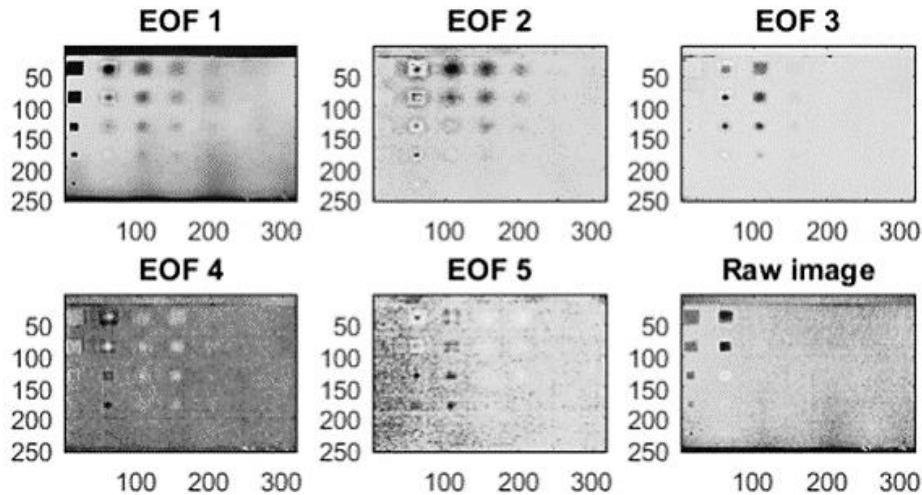
Figure 4. Different components obtained through PCT

Table 3. Different principal components obtained after applying PCT

Sl. No.	Defect	SNR (dB)					
		Raw Image	EOF 1	EOF 2	EOF 3	EOF 4	EOF 5
1.	R1C2	32.09	56.382	39.378	39.368	43.669	35.288
2.	R2C2	33.09	61.486	45.451	40.381	45.032	35.314
3.	R1C3	31.48	58.098	44.312	41.922	42.895	33.700
4.	R2C3	18.63	59.561	46.183	44.597	43.606	34.660
5.	R1C4	14.75	55.890	44.763	44.403	41.817	32.928
6.	R2C4	7.92	63.898	47.653	47.882	44.292	35.268

4.6. Partial least square regression (PLSR)

Figure 5 provides the PLS components of the defects considered for the experiment. The SNR values of six defects were tabulated for the first six PLS components in Table 4 and then compared with the SNR values of the defects in the raw image. It is observed that various defect depths achieve maximum SNR in different PLS components.
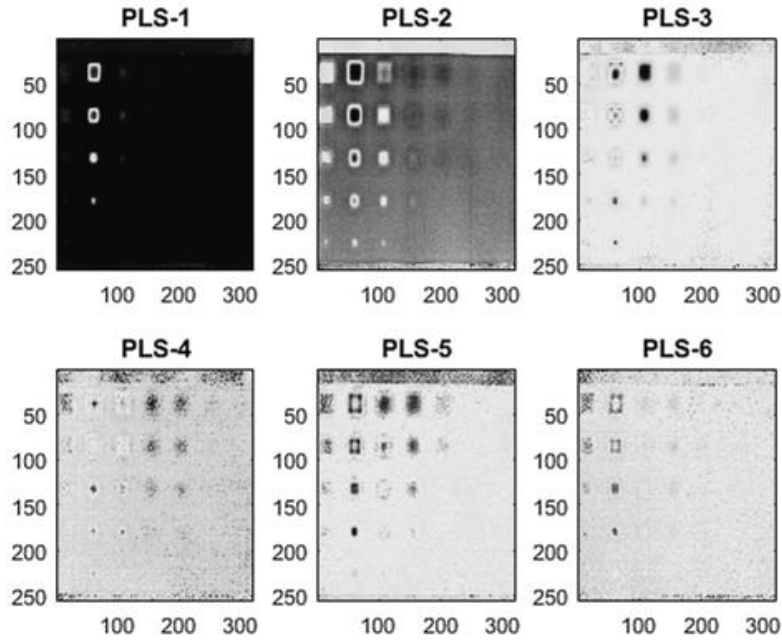
Figure 5. Different PLS components obtained after applying PLSR

Table 4. SNR values of different defects for varying PLS components

Sl. No.	Defect	SNR (dB)						
		Raw Image	PLS 1	PLS 2	PLS 3	PLS 4	PLS 5	PLS 6
1.	R1C2	32.09	53.77	40.09	25.26	5.89	23.55	13.47
2.	R2C2	33.09	54.27	38.94	10.18	2.86	23.92	13.66
3.	R1C3	31.48	44.94	16.85	31.35	2.32	19.84	2.20
4.	R2C3	18.63	33.41	26.57	29.62	8.63	11.44	7.69
5.	R1C4	14.75	46.25	19.86	23.38	15.81	20.61	3.60
6.	R2C4	7.92	54.84	6.14	23.22	14.43	18.06	4.72

4.7. Autoencoder based approach

The tradeoff considered in this work is SNR improvement vs defect visibility. The autoencoder architecture is capable of providing output images with higher SNR, though the defects may not be visible always. Depending on the requirements or specifications, the parameters defined for the neural network is varied to maximize either SNR or defect visibility. The reconstructed images for R1C2 defect for varying SNR are shown in Figure 6. The images in Figure 6(a) to Figure 6(i) are the reconstructed outputs from randomly sampled input thermal images. The changes in SNR obtained during different epochs of training the autoencoder is presented in Figure 7 and maximum SNR obtained is tabulated in Table 5.

Neural networks perform very well in optimizing an objective function. In this case, the network is trained to reconstruct the images. The non-linearity of the model and differing statistics of the training data ensure that the reconstructed image is not a copy of the input. This is utilised to select the parameters for which the reconstructed images provide a higher SNR and have good amount of defect visibility. This has a drawback of not providing the best or optimum performance unless fine tuned.

4.8. Comparison of SNR for different methods

The performance of defect detection is compared in terms of SNR obtained by different methods and tabulated in Table 6. From the table it is observed that PCT performs better than other signal processing algorithms in terms of SNR increase. The proposed deep learning architecture based autoencoder exhibits the best SNR for all the defects. As shown in the table, reconstructed images from randomly sampled input thermal images exhibit a higher SNR for the proposed autoencoder architecture compared to other signal processing approaches. This observation shows promise on how further research in this area on customised algorithms and objective functions can result in optimal performance without any fine-tuning.
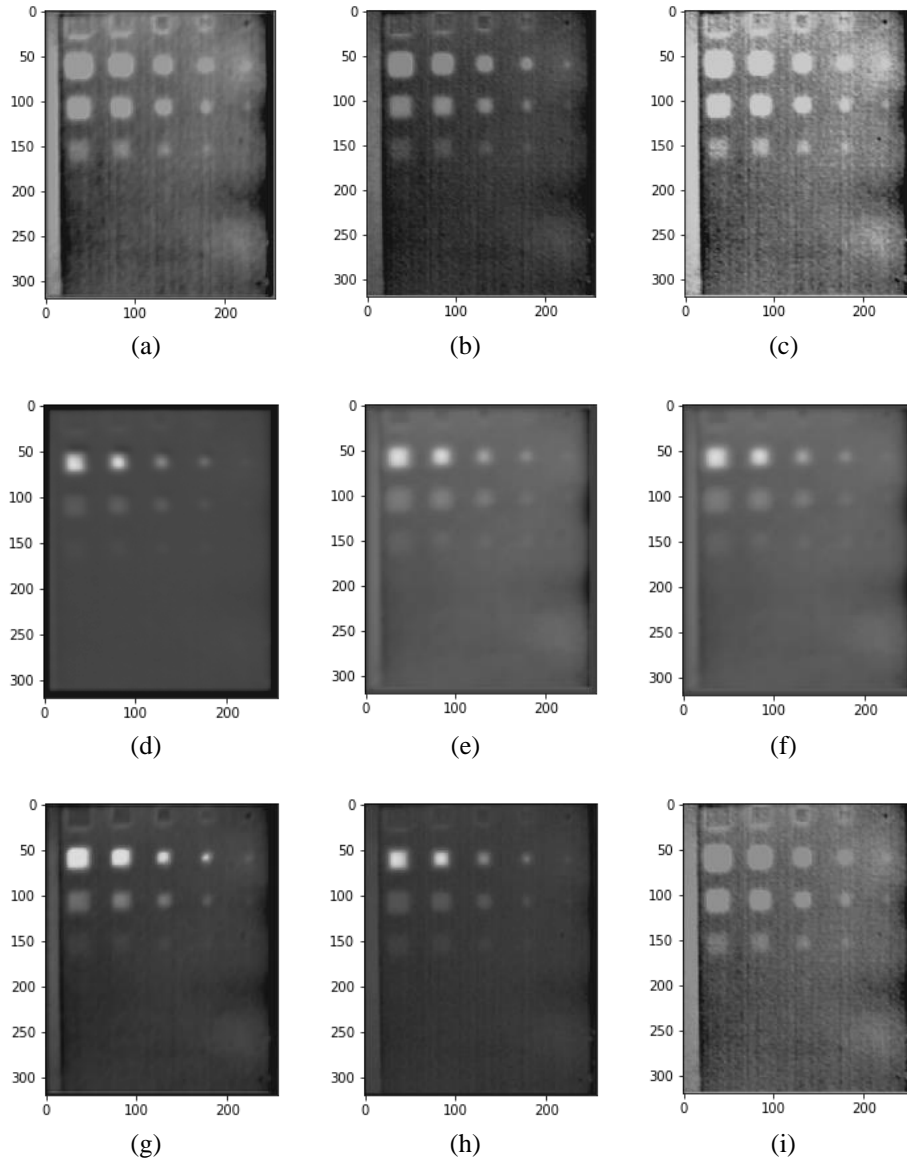
Figure 6. Reconstructed images for R1C2 defect with varying SNR (a) SNR=32.04 dB, (b) SNR=40.17 dB, (c) SNR=120.82 dB, (d) SNR=42.73 dB, (e) SNR=124.08 dB, (f) SNR=37.38 dB, (g) SNR=117.84 dB, (h) SNR=39.08 dB, and (i) SNR=38.06 dB
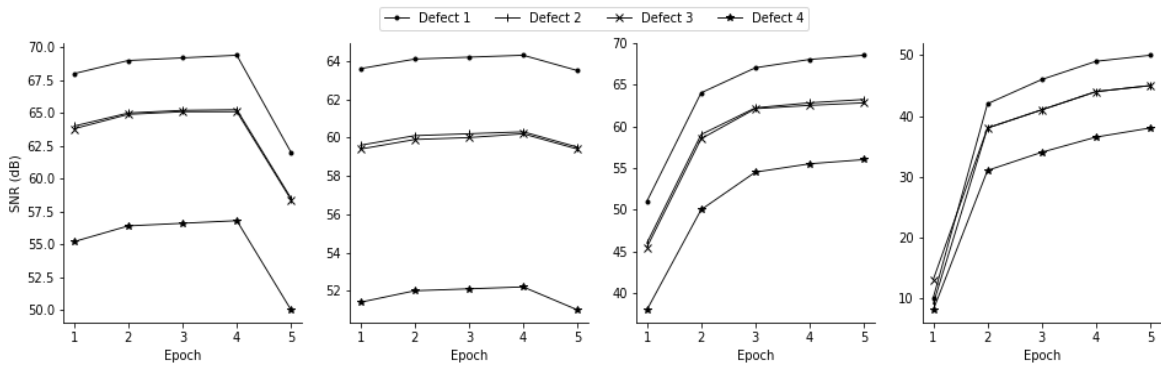

Figure 7. SNR (dB) variation for various defects

Table 5. Maximum SNR values of different defects

Sl. No.	Defect	SNR (dB)	
		Raw Image	AE
1.	R1C2	32.09	65.180
2.	R2C2	33.09	73.430
3.	R1C3	31.48	73.120
4.	R2C3	18.63	77.670

Table 6. SNR in dB of different algorithms

Sl. No.	Defect	SNR (dB)				
		Raw Image	HOS	PCT	PLSR	AE
1.	R1C2	32.09	37.346	56.382	53.770	65.180
2.	R2C2	33.09	27.611	58.098	44.940	73.430
3.	R1C3	31.48	36.877	61.486	54.270	73.120
4.	R2C3	18.63	11.198	59.561	33.410	77.670

5. CONCLUSION

The evaluation and extensive analysis of standard signal processing approaches provided a good baseline for SNR improvement and defect visibility. HOS not being used for defect visualization improved the SNR of the defects. PCT displayed considerable contrast enhancement between defect and non-defect regions which led to better defect visualization and higher SNR values as compared to other algorithms. PLSR provided the best performance among all the algorithms in terms of SNR improvement, defect visibility and contrast enhancement. The proposed autoencoder architecture-based algorithm performs better than signal processing approaches with noticeable increase in SNR. It improves defect visibility in some cases and this can be attributed to embedding the input data into higher dimensions using convolution kernels and using non-linear activation functions in this space. During reconstruction, activation function is used only at the last layer to normalise the output. The advantage is that large convolution filters are not necessary for this task. This is due to the fact that representation in a higher dimensional space is more important than learning large dimensions spatial information for this task. This network when optimised can represent and reconstruct any given image effectively. It also helps in data compression with the architecture able to learn the important features. Some of the limitations of this algorithm is that neural network architectures do not perform well with distribution shift, i.e., when the test set is statistically very different from the training set. Normalization or adaptative algorithms may ensure that test data is similar to the data the model is trained on. These models are still in its nascent stage compared to signal processing approaches and neural networks are indeed a high dimensional learnable black-box function, and so the generated models are not explainable. To conclude, signal processing and neural network based algorithms provide a set of tools to increase the SNR, enhance defect visibility and provide data compression in many applications for thermal imaging of stainless steel material with PT approach. Neural network architectures show a lot of promise for this application. Emerging neural network-based approaches such as generative adverserial networks (GANs), variational autoencoders (VAE) and attention-based networks can be considered to represent thermal images for better SNR and defect visibility as compared to autoencoders.

REFERENCES

[1] S. K. Lau, D. P. Almond, and J. M. Milne, "A quantitative analysis of pulsed video thermography," *NDT E Int.*, vol. 24, no. 4, pp. 195–202, Aug. 1991, doi: 10.1016/0963-8695(91)90267-7.

[2] X. Maldague, *Theory and practice of infrared technology for non-destructive testing*. Wiley-Interscience, 2001.

[3] F. J. Madruga, C. Ibarra-Castanedo, O. M. Conde, J. M. López-Higuera, and X. Maldague, "Infrared thermography processing based on higher-order statistics," *NDT E Int.*, vol. 43, no. 8, pp. 661–666, Nov. 2010, doi: 10.1016/j.ndteint.2010.07.002.

[4] S. M. Shepard, "Reconstruction and enhancement of active thermographic image sequences," *Opt. Eng.*, vol. 42, no. 5, May 2003, doi: 10.1117/1.1566969.

[5] N. Rajic, "Principal component thermography for flaw contrast enhancement and flaw depth characterisation in composite structures," *Compos. Struct.*, vol. 58, no. 4, pp. 521–528, Dec. 2002, doi: 10.1016/S0263-8223(02)00161-7.

[6] F. Lopez, C. Ibarra-Castanedo, V. de Paulo Nicolau, and X. Maldague, "Optimization of pulsed thermography inspection by partial least-squares regression," *NDT E Int.*, vol. 66, pp. 128–138, Sep. 2014, doi: 10.1016/j.ndteint.2014.06.003.

[7] P. Bison, C. Bressan, R. Di Sarno, E. Grinzato, S. Marinetti, and G. Manduchi, "Thermal NDE of delaminations in plastic materials by neural network processing," 1994., doi: 10.21611/qirt.1994.032.

[8] H. Trétout, D. David, J. Y. Marin, M. Dessendre, M. Couet, and I. Avenas-Payan, "An evaluation of artificial neural networks applied to infrared thermography inspection of composite aerospace structures," in *Review of Progress in Quantitative Nondestructive Evaluation*, Boston, MA: Springer US, 1995, pp. 827–834., doi: 10.1007/978-1-4615-1987-4_103.

[9] G. Manduchi, S. Marinetti, P. Bison, and E. Grinzato, "Application of neural network computing to thermal non-destructive evaluation," *Neural Comput. Appl.*, vol. 6, no. 3, pp. 148–157, Sep. 1997, doi: 10.1007/BF01413826.

[10] M. B. Saintey and D. P. Almond, "An artificial neural network interpreter for transient thermography image data," *NDT E Int.*, vol. 30, no. 5, pp. 291–295, Oct. 1997, doi: 10.1016/S0963-8695(96)00071-0.

[11] S. Vallerand and X. Maldague, "Defect characterization in pulsed thermography: a statistical method compared with Kohonen and perceptron neural networks," *NDT E Int.*, vol. 33, no. 5, pp. 307–315, Jul. 2000, doi: 10.1016/S0963-8695(99)00056-0.

[12] A. Darabi and X. Maldague, "Neural network based defect detection and depth estimation in TNDE," *NDT E Int.*, vol. 35, no. 3, pp. 165–175, Apr. 2002, doi: 10.1016/S0963-8695(01)00041-X.

[13] N. Saeed, M. A. Omar, and Y. Abdulrahman, "A neural network approach for quantifying defects depth, for non-destructive testing thermograms," *Infrared Phys. Technol.*, vol. 94, pp. 55–64, Nov. 2018, doi: 10.1016/j.infrared.2018.08.022.

[14] N. Saeed, N. King, Z. Said, and M. A. Omar, "Automatic defects detection in CFRP thermograms, using convolutional neural

networks and transfer learning," *Infrared Phys. Technol.*, vol. 102, Nov. 2019, doi: 10.1016/j.infrared.2019.103048.

[15] D. Müller, U. Netzelmann, and B. Valeske, "Defect shape detection and defect reconstruction in active thermography by means of two-dimensional convolutional neural network as well as spatio-temporal convolutional LSTM network," *Quant. Infrared Thermogr. J.*, vol. 19, no. 2, pp. 126–144, 2022, doi: 10.1080/17686733.2020.1810883.

[16] N. Saeed, H. Al Zarkani, and M. A. Omar, "Sensitivity and robustness of neural networks for defect depth estimation in CFRP composites," *J. Non-destructive Eval.*, vol. 38, no. 3, Sep. 2019, doi: 10.1007/s10921-019-0607-4.

[17] Y. Duan *et al.*, "Automated defect classification in infrared thermography based on a neural network," *NDT E Int.*, vol. 107, Oct. 2019, doi: 10.1016/j.ndteint.2019.102147.

[18] C. Xu, J. Xie, C. Wu, L. Gao, G. Chen, and G. Song, "Enhancing the visibility of delamination during pulsed thermography of carbon fiber-reinforced plates using a stacked autoencoder," *Sensors*, vol. 18, no. 9, Aug. 2018, doi: 10.3390/s18092809.

[19] Y. He *et al.*, "Infrared machine vision and infrared thermography with deep learning: a review," *Infrared Phys. Technol.*, vol. 116, Aug. 2021, doi: 10.1016/j.infrared.2021.103754.

[20] Z. Wei, H. Fernandes, H.-G. Herrmann, J. R. Tarpani, and A. Osman, "A deep learning method for the impact damage segmentation of curve-shaped CFRP specimens inspected by infrared thermography," *Sensors*, vol. 21, no. 2, Jan. 2021, doi: 10.3390/s21020395.

[21] Q. Fang, C. Ibarra-Castanedo, and X. Maldague, "Automatic defects segmentation and identification by deep learning algorithm with pulsed thermography: synthetic and experimental data," *Big Data Cogn. Comput.*, vol. 5, no. 1, Feb. 2021, doi: 10.3390/bdcc5010009.

[22] N. Saeed, Y. Abdulrahman, S. Amer, and M. A. Omar, "Experimentally validated defect depth estimation using artificial neural network in pulsed thermographyy," *Infrared Phys. Technol.*, vol. 98, pp. 192–200, May 2019, doi: 10.1016/j.infrared.2019.03.014.

[23] P. Kovács, B. Lehner, G. Thummerer, G. Mayr, P. Burgholzer, and M. Huemer, "Deep learning approaches for thermographic imaging," *J. Appl. Phys.*, vol. 128, no. 15, Oct. 2020, doi: 10.1063/5.0020404.

[24] Q. Fang and X. Maldague, "Defect depth estimation in infrared thermography with deep learning," in *3rd International Symposium on Structural Health Monitoring and Non-destructive Testing*, 2020, pp. 1–12.

[25] Q. Luo, B. Gao, W. L. Woo, and Y. Yang, "Temporal and spatial deep learning network for infrared thermal defect detection," *NDT E Int.*, vol. 108, p. 102164, Dec. 2019, doi: 10.1016/j.ndteint.2019.102164.

BIOGRAPHIES OF AUTHORS

Sethu Selvi Selvan (iD) (g) (SC) (P) Professor, Department of ECE, Ramaiah Institute of Technology obtained her Ph.D. from Indian Institute of Science in 2001 under Prof. Anamitra Makur in the area of Image Compression. She completed her B.E. from Thiagarajar College of Engineering, Madurai in 1992 and M.E. from Anna University in 1994. She joined the Faculty of Department of Electronics and Communication at M.S. Ramaiah Institute of Technology, Bangalore, in 2002 as Assistant Professor. She has numerous publications to her name in the field of Machine Learning, Pattern Recognition and Signal and Image Processing. Her fields of interests are Digital Image Processing, Machine/Deep Learning, Video Processing, Character Recognition and Biometrics. She has authored a chapter titled "Image Algebra and Image Fusion" in the book "Data Fusion Mathematics: Theory and Practice", CRC Press, 2017 and has been listed as a noteworthy technical contributor by Marquis Who's Who (World), 2009. She can be contacted at email: selvi@msrit.edu.

Sharath Delanthabettu (iD) (g) (SC) (P) is working as Research Scientist in Center for Imaging Technologies at M.S. Ramaiah Institute of Technology, Bengaluru. He has obtained his Ph.D. from Homi Bhabha National Institute, IGCAR Kalpakkam Campus in 2015. He is working in the areas of Infrared Imaging and its applications in Non-Destructive Evaluation and health care, and image processing. He has published 18 articles in international and national journals. He can be contacted at email: sharathd@msrit.edu.

Menaka Murugesan (iD) (g) (SC) (P) is a postgraduate in Physics and has over 19 years of experience in the field of NDE for materials characterization. She has specialized in the areas of thermal imaging, image processing and digital radiography. She is presently heading Radiation Application and Metrology section at Radiological Safety Division of IGCAR, Kalpakkam. Her field of interests are material characterization using thermal NDE and thermal imaging as diagnostic tool in healthcare. She is an American Society for NDT certified Level – III in Infrared Thermal Testing. She can be contacted at email: menaka@igcar.gov.in.

Venkatraman Balasubramaniam is Distinguished Scientist and Director of IGCAR, Kalpakkam and CMD of BHAVINI, Kalpakkam. He post-graduated in Physics from St. Joseph College (Autonomous), Tiruchirappalli and obtained his Ph. D from Madras University. With a research career spanning 37 years, he has combined the physics of Non-Destructive Evaluation (NDE) with engineering and technology and consistently provided excellent R & D support and robust NDE-based solutions to technologically challenging problems in nuclear and other strategic and core industries. His significant milestone activities for the nuclear industry include - Procedures for X-ray and neutron radiography of highly irradiated fuel pins, comprehensive NDE for evaluation of tube-to-tube sheet welds of PFBR steam generator and radiometric testing of shielding structures. He has been primarily responsible for establishing the conventional and digital X-ray, neutron radiography and thermal imaging facilities at IGCAR. He is recipient of various prestigious awards and fellowships. He can be contacted at email: bvenkat@igcar.gov.in.

Sathvik Udupa is working as a Research Associate in Indian Institute of Science (IISc), Bangalore. He obtained his B.E. from Ramaiah Institute of Technology, 2019. He is working in the areas of speech recognition, speech synthesis and multimodal machine learning. He can be contacted at email: sathvikudupa66@gmail.com.

Tanvi Khandelwal graduated in Electronics and Communication from Ramaiah Institute of Technology, Bangalore in 2019. She is working as ATC Application Design Engineer in Alstom, Bangalore. Her interests are in image processing and AI. She can be contacted at email: tanvi.khandelwal717@gmail.com.

Touqueer Mulla graduated in Electronics and Communication from Ramaiah Institute of Technology, Bangalore in 2019. He is working as Program Analyst for Cognizant, India. His interests are in AI and embedded systems. He can be contacted at email: touqeer.004@gmail.com.

Varun Ittigi graduated in Electronics and Communication from Ramaiah Institute of Technology, Bangalore in 2019. He has worked in Innocirc Ventures as an Artificial Intelligence Research Engineer. His interests are in AI and Robotics. He can be contacted at email: varunittigi10@gmail.com.